Journal of Catalysis 413 (2022) 1123–1131

Contents lists available at ScienceDirect

Journal of Catalysis

journal homepage: www.elsevier.com/locate/jcat

Disentangling catalysis and mass transport: Using diffusion measurements by pulsed field gradient NMR to reveal the microkinetics of CO oxidation over nanoporous gold

Amineh Baniani [a,1], Stefan Wild [b,c,1], Evan M. Forman [a], Thomas Risse [d], Sergey Vasenkov [a], Marcus Bäumer [b,c,*]

[a] Department of Chemical Engineering, University of Florida, Gainesville, FL 32611, USA
[b] Institute for Applied and Physical Chemistry, University of Bremen, 28359 Bremen, Germany
[c] MAPEX Center of Materials and Processes, University of Bremen, 28359 Bremen, Germany
[d] Institute of Chemistry and Biochemistry, Free University Berlin, 14195 Berlin, Germany

ARTICLE INFO

Article history:
Received 24 June 2022
Revised 12 August 2022
Accepted 16 August 2022
Available online 19 August 2022

Keywords:
Nanoporous metals
Au catalysts
Diffusive mass transport
Low temperature CO oxidation
Macrokinetics
Microkinetics
PFG NMR

ABSTRACT

Since the first studies reporting on its surprising catalytic properties, nanoporous gold (npAu) has emerged as a novel and ever since intensively investigated type of Au based catalyst. To judge its genuine catalytic potential and to be able to optimize its use in applications, it is mandatory, however, to quantify the influence of mass transport in the porous structure on the observed catalytic rates, i.e., to study the interplay between diffusion and reaction. To this end, we used pulsed field gradient (PFG) NMR for the first time to directly determine the diffusivities of reaction gases in a nanoporous metal – in this case for CO and CO_2 as species involved in low temperature CO oxidation efficiently catalyzed by npAu. By comparing the diffusion coefficients within the 20 nm pores of the material with the values in the bulk gas phase, the tortuosity of npAu's pore system was assessable as the central geometrical parameter describing the extent to which diffusive transport in the pore system is slowed down. This knowledge allowed us in the following to disentangle the contributions of mass transport and the kinetics of the surface reaction (microkinetics). In particular, we were able to determine the rate constant and turnover frequency for low-temperature CO oxidation without previous ambiguities arising from potential transport limitations and to compare the results with other reported values. Based on the results, it was furthermore possible to predict optimized dimensions of the catalyst, resulting in minimized or even suppressed diffusion limitations. These predictions could be successfully verified, using np-Au platelets with lateral dimensions in the range of a few hundred microns. In this way, the catalytic conversion could be ramped up by 50 % and an activity level advanced which reflected the microkinetic potential of np-Au.

1. Introduction

Nanoporous gold emerged in 2006 as a new type of Au catalyst not known before and being structurally distinct from supported Au catalysts which had been in the focus of research before [1,2]. The material, representing, like Raney nickel, a skeletal metal catalyst, is obtained as the result of a corrosive dealloying process, during which a less noble sacrificial metal – usually silver – is leached out of an alloy with Au chemically or electrochemically [3]. Already in the first studies dealing with the oxidation of CO, npAu had been found to efficiently catalyze aerobic oxidation reactions at room temperature and even below [1,2]. Later, also npAu's ability to catalyze partial oxidation reactions with high selectivity was exemplified for methanol oxidation to methylformate [4].

In the case of Au nanoparticles (NP), typically only a narrow range of particle sizes around a few nm shows catalytic activity for which also the type of oxide used as a support plays a decisive role [5]. In contrast, npAu exhibits pores and ligaments, i.e., structural features, which are about an order of magnitude larger (typically 20–50 nm) than their nanoparticulate counterparts [6]. The high activity and selectivity of this seemingly pure Au catalyst attracted considerable attention and led to many research activities which ever since have documented npAu's catalytic potential for a variety of reactions in gas as well as in liquid phase [3,7,8]. Even though it meanwhile turned out that the notion of npAu being a pure Au catalyst is wrong and residues of the sacrificial

* Corresponding author.
E-mail address: mbaeumer@uni-bremen.de (M. Bäumer).
[1] These authors contributed equally to the work.

https://doi.org/10.1016/j.jcat.2022.08.020
0021-9517/

metal (such as Ag) have been identified to play an important part as well [9,10], the material holds great promises in particular as an oxidation catalyst, performing already at temperatures where Pt and other established metals not yet work.

Two factors, though, hampered a concluding judgement of npAu's catalytic potential - also in view of technical applications – and a well-founded comparison with other types of Au catalysts so far. The first one relates to its activation. Taking CO oxidation as an example of a frequently studied reaction in the area of Au catalysis, the synopsis of previous work suggests that npAu not always displays activity directly after preparation, but rather evolves it slowly over time [11–13]. For this total oxidation reaction, we recently found that short-term annealing treatments to 300 °C in the reaction gas mixture provide a reliable means to reach high catalytic activity quickly and reproducibly, while retaining the surface area of the porous structure [14]. Yet, for the wealth of reactions catalyzed by npAu the microscopic details of the underlying active surface states still are a matter of intense research and thus are robust procedures of evoking them [8]. The other factor not sufficiently clarified up to now relates to the quantitative assessment of mass transport limitations, resulting from npAu's pore structure. Such knowledge not only is necessary for an unambiguous evaluation of npAu's intrinsic catalytic capabilities (in terms of TOFs, i.e., turnover frequencies, for instance), but also constitutes a prerequisite for reducing such contributions and thus optimizing the catalytic productivity in any kind of application.

It was early speculated that npAu's ubiquitous mesoporosity could indeed pose a serious impediment for exploiting the full catalytic potential of npAu [12]. In particular, in case of larger monoliths, being the typical kind of specimen obtained by established protocols for preparing npAu by dealloying, the lack of larger macropores, which have an ability of facilitating the mass transport into deeper sections of the material, could render major parts of the material catalytically unused. In fact, preliminary studies on low temperature CO oxidation suggested that under unfavorable conditions as far as the tortuosity and the connection of the pores is concerned a severe productivity cut-off is not unlikely, which would make large scale applications unattractive in view of Au's high market prices [12,15]. Precise assessments, however, were baffled due to lacking precise quantitative knowledge about npAu's transport properties.

Dealing with mass transport in porous matter where molecular confinement plays a decisive role, *two* factors have to be taken into account, altering and limiting the diffusive transport as compared to the bulk gas phase [16]. On the one hand, molecular diffusion turns into Knudsen diffusion when the mean free path of the molecules exceeds the pore diameters so that collisions with their walls become more likely than intermolecular collisions. This aspect is less of a problem, as diffusion constants in the Knudsen regime can be derived on the basis of (mean) pore diameters as obtainable e.g from SEM micrographs [17]. Even when both mechanisms – Knudsen and molecular - contribute, the resulting transition regime can be accounted for by reverting to the so-called Bosanquet equation ($1/D_T = 1/D_{molecular} + 1/D_{Knudsen} = 1/D_M + 1/D_K$) [17]. The second factor, however, is material specific and not assessable on the basis of general principles. It results from the elongation of the diffusive pathways enforced by the particular pore system under consideration [18]. A parameter that was introduced to integrally characterize this structurally caused impact is the so-called tortuosity factor τ [16]. It needs to be experimentally determined either on the basis of structural information or measurements of the gas diffusivities within the material [19,20].

Embarking on the latter strategy, we took advantage of pulsed field gradient (PFG) NMR and its far-reaching capabilities to study diffusion of gases not only in the bulk phase but also in porous materials to get quantitative insight into the transport properties of npAu [21]. In case of micro- and mesoporous oxides the method has already contributed tremendously to our understanding of diffusive transport in porous matter [16,18]. Notably, PFG NMR and NMR relaxometry have also been applied successfully to study diffusion and dynamics in supported metal and also supported gold catalysts [22–24]. Porous metals, such as npAu, however, have not been the subject of corresponding experiments so far – perhaps because of concerns that eddy currents induced in the metallic framework could prevent meaningful experiments by PFG NMR. Herein, we show the applicability of the technique also for this class of systems by determining the diffusivities of CO and CO_2, i.e., the educt and the product of CO oxidation, in the pore system of npAu.

Deriving diffusivities from such data of course requires short contact times of the investigated molecules with the pore walls. In other words, the corresponding residence times on the surface have to be sufficiently short as compared to the time scale of the experiment to assure that the results not only cover a fraction of the diffusing gas ensemble [20,24]. Since CO oxidation is known to follow a Langmuir-Hinshelwood mechanism [25], the educts and products, however, must be trapped on the surface at least for some time so that this question clearly is of relevance in the present case and needs to be addressed beforehand. In this context, experimental knowledge about the adsorption properties of the involved gases on Au surfaces provides a basis to dispel corresponding concerns.

In case of CO, for example, temperature programmed desorption (TPD) experiments carried out under UHV conditions revealed desorption temperatures, ranging from 120 K to ~220 K for npAu [26]. These values indicate binding energies between ~0.4 and 0.6 eV (assuming a typical preexponential factor of 10^{13} s^{-1}) – in contrast to flat defect-free Au(1 1 1) surfaces, where the molecule is known to be much weaker bound (~0.3 eV) [27]. It was thus concluded and also corroborated by theoretical calculations that the higher binding energies belong to defect sites, which were found to make up a share of 20 % of npAu's surface atoms [28] and to act as primary adsorption (and probably reaction) sites for CO on this catalyst [29]. In spite of this comparatively high number, only chemisorption on those surface sites exhibiting the highest binding energies will lead to residence times that come close to the studied diffusion times (6–30 ms). Their fraction, however, is low enough to ensure that the number of CO molecules trapped there on their diffusive pathway inside the material is sufficiently small. In accord, for CH_4, included in our study as an inert molecule which neither chemisorbs nor reacts on Au surfaces, very similar results were obtained by PFG NMR.

CO_2 as the product, is known to exhibit low binding energies on Au as well [30] so that it desorbs from the surface once it is formed. Accordingly, its diffusive transport out of the pores into the bulk gas phase is not likely to mitigate the catalytic conversion. This conclusion also holds true for O_2, i.e., the other reactant of CO oxidation. Here, previous kinetic studies revealed reaction orders close to zero [12,31], implying that, in contrast to CO, where reaction orders close to 1 were typically found, the supply of oxygen at the surface represents no limiting factor for the kinetics and thus for the mass transport in case of CO oxidation over npAu.

Based on the PFG NMR results obtained for the studied gases, we were therefore in the position to determine the tortuosity factor of npAu's pore structure for the first time experimentally, revealing that the resistance posed for diffusive transport is less pronounced than previously assumed [12]. This knowledge allowed in a second step to determine the effective diffusion coefficient of CO within the material, as the kinetically governing reactant for its catalytic conversion to CO_2 at 30 °C and under ambient pressure. By employing the Thiele modulus concept as an established formalism in chemical engineering to evaluate catalyst effi-

ciencies (macrokinetics) [32], resulting from the interplay of catalytic turnover at the surface (microkinetics) and diffusive mass transport, it was possible to disentangle the macro- and microkinetics for this reaction. To make sure that the data revealed in this way reflect the catalytically most active state of the surface, we took advantage of an activation procedure, for which we recently showed that it ensures achieving maximal CO conversion levels for npAu [14].

The quantitative knowledge about the transport properties, on the one hand, and the microkinetics of the surface reaction under consideration, on the other hand, lays the foundation for strategies aiming at optimizing the productivity in any kind of catalytic application. When the structure of the pore system itself cannot easily be adjusted to minimize mass transport limitations, changing the shape and size of the catalyst can provide an alternative option in this respect. In a first attempt to exemplify this approach, we compared larger monolithic npAu discs - as a sample type often employed in the past - with smaller platelets which exhibited the same thickness (200 μm) but diameters that were an order of magnitude smaller (a few 100 μm as compared to a few mm). The conversion gain achieved in this way quantitatively reflected the prediction made on the basis of npAu's experimentally determined tortuosity and the microkinetics, thus confirming the consistency of the data set.

2. Experimental

2.1. Preparation of npAu samples

Nanoporous gold was prepared by leaching silver out of an AgAu alloy in conc. HNO_3 – a dealloying process called "free corrosion". The AgAu starting alloy was fabricated by alloying gold (Chempur, 99.999 %) and silver (Chempur, 99.99 %) in a ratio of 30.00 ± 0.03 at% Au and 70.00 ± 0.03 at% Ag at 1100 °C for 30 min (initial heating rate: 0.2 °C/s) in a boron nitride crucible (Situs, purity: 99.9 %). The resulting alloy was subsequently cooled down to room temperature (0.2 °C/s) and traces of boric acid deposited on the surface of the obtained ingots were removed with 1 M citric acid (Sigma-Aldrich, 99.5 %) at 50 °C for 30 min. Before further processing, the material was homogenized at 875 °C in a tube furnace under an argon atmosphere (Linde, 99.999 %, flow: 20 sccm) for 120 h.

To obtain suitable specimen for the PFG NMR and the catalytic experiments, thin sheets of the starting alloy were prepared by using an adjustable roller and applying several cold rolling steps. In each step the reduction of thickness was limited to 20 % to minimize the associated mechanical stress which was subsequently dissipated by annealing the material in a furnace at 400 °C for 15 min. After 5–6 passes, alloy sheets with a nominal thickness of ~200 μm were finally obtained. For the PFG NMR measurements discs of about 3 mm were punched out of such sheets, whereas the disc diameters amounted to 5 mm in case of the catalytic investigations.

For dealloying, the samples were put on a porous (250–500 μm) borosilicate disc, which, in turn, was placed in a 100 ml beaker. Subsequently, the specimen were immersed in 50.0 ml conc. HNO_3 (Merck, ≥65%, p.a.) for 18–24 h and then washed three consecutive times for 1 min with 100 ml deionised water. Overall, the preparation followed established protocols, as for example described in Ref. [14], yielding a mean ligament diameter of $\langle d_l \rangle$ = 18 nm ± 4.2 nm in the present case (as determined by a careful Fourier analysis of acquired SEM micrographs).

To break up the monolithic npAu discs into entities with smaller lateral dimensions, we developed a mechanical method based on shaking them in a closed glass vial for several min. To this end, we took advantage of the grain microstructure of the polycrystalline material and its propensity to show predominant fracture at associated grain boundaries. The platelets obtained in this way exhibited a thickness identical with the former discs (200 μm) but were broken down to lateral dimensions being an order of magnitude smaller than the previous disc diameters (a few 100 μm vs. a few mm). Since the grain structure and thus particle sizes assessable by this strategy are determined by the cold rolling process and the intermittent annealing steps, they are susceptible to manipulation, bearing the opportunity to tune their mean size and to optimize the size distribution. Exploring this potential, however, was beyond the scope of the present study. In any event, it entails the advantage of not damaging the porosity - in contrast to previously described methods in the literature that were based, e.g., on piercing and disrupting samples with a needle or a pincer [33].

2.2. PFG NMR measurements

The npAu gold discs prepared for the NMR measurements were stacked on top of each other inside a 5 mm (medium walled) NMR tube (Wilmad Labglass, Inc.), reaching a height of 28 ± 3 mm. The tube was attached to a custom-made vacuum system and exposed to high vacuum at room temperature overnight, enabling the removal of any sorbates present in the sample. Subsequently, sorbate loadings were performed. The sorbates used for this study were ^{13}C-enriched carbon monoxide (CO) exhibiting 99 % isotopic purity (Sigma-Aldrich), ^{13}C-enriched methane (CH_4) with 99 % isotopic purity (Sigma-Aldrich), and ^{13}C-enriched carbon dioxide (CO_2) with 99 % isotopic purity (Sigma-Aldrich). A known mass of the ^{13}C-labelled sorbate was transferred cryogenically into the NMR tubes containing the nanoporous gold particles. Upon the sorbate loadings were accomplished, the tubes were flame-sealed. The sorbate loadings in each sample were checked in the same way as discussed in Ref. [34]. In all cases a pressure of 15 bar corresponding to gas loadings of 0.11 ± 0.02 mmol/g(npAu) was used. For CO_2, in addition, a lower loading was prepared and measured to confirm that the tortuosity factor of npAu derived from the PFG NMR data does not depend on the sorbate concentration (see SI).

PFG NMR diffusion measurements and NMR relaxation measurements were subsequently performed with a 17.6 T Avance III HD spectrometer (Bruker Biospin), operating at a resonance frequency of 188.6 MHz for ^{13}C. For methane, additional PFG NMR diffusion measurements and NMR relaxation measurements were carried out at a proton resonance frequency of 750 MHz, using the same spectrometer. Sine-shaped, bipolar magnetic field gradients with an effective duration of 0.15 ms and amplitudes up to 5 T/m were generated, using a DIFF50 diffusion probe (Bruker BioSpin). For the diffusion measurements, the 13-interval PFG NMR pulse sequence with bipolar gradients was employed[35], modified by the addition of a longitudinal eddy current delay of about 5 ms. Longitudinal (T_1) and transverse (T_2) relaxation times were measured, using standard inversion recovery and Carr-Purcell-Meiboom-Gill (CPMG) pulse sequences, respectively. The delay time in the CPMG sequence was equal to 100 μs. All NMR measurements reported in this work were performed at 23 °C.

Gas diffusivities were obtained from the measured PFG NMR attenuation curves, i.e., dependences of the PFG NMR signal intensity on the effective magnetic field gradient strength, with all other pulse sequence parameters held fixed. The PFG NMR signal intensities were derived by integration of the corresponding NMR spectra (see SI). Under our measurement conditions, the ^{13}C NMR spectra of CO, CH_4, and CO_2 consisted of just a single line at around 184, −10.6, and 126 ppm, respectively, and the ^{1}H NMR spectra recorded for CH_4 of a single line at around 2.6 ppm. In more detail, the data evaluation is described in the SI.

2.3. Catalytic measurements

The npAu discs employed in the catalytic measurements were placed in a quartz tube reactor (8 mm inner diameter) by sandwiching them in the middle of the tube between 4 cm quartz sand (Roth, grain size: 700–800 μm, calcined at 1000 °C for 10 h) which, in turn, was held in place by quartz wool plugs (Roth, pure). The reactor was inserted in a tube furnace controlled by a Eurotherm PID device for heating. As detailed elsewhere, the reactor could be cooled down quickly on demand by injecting compressed air into the space between the reactor tube and the furnace [14].

The catalytic CO oxidation experiments were carried out, using a reaction mixture of 89.0 vol% Helium (5.0 Linde, 99.999 %), 1.0 vol % carbon monoxide (5.0 Linde, 99.999 %) and 10.0 vol% oxygen (5.0 Linde, 99.999 %), i.e., in an excess of oxygen. The composition was adjusted by mass flow controllers (GE50A, MKS instruments, backpressure: 3.5 bar) and allowed to stabilize in a reactor bypass, before admitting it to the reactor. The total gas flow used for all experiments amounted to Q_T^0 = 40 ml/min. (Note that the gas flows regulated by the mass flow controllers and thus also the total flow refer to standard conditions: 0 °C and 1000 mbar.)

The npAu samples were catalytically activated, using an optimised version of a recently published activation protocol for CO oxidation. In this way, the reliable and reproducible achievement of high and sustainable conversion levels at 30 °C could be ensured within one hour or less [14]. To this end, the samples were quickly heated (heating ramp: ~1 °C/s) five consecutive times to 300 °C, holding this temperature for 90 s and subsequently cooling the reactor down to 30 °C again (cooling rate: ~0.7 °C/s). It was previously shown that this procedure does not affect the pore structure.

The effluent gas mixture leaving the reactor was continuously analysed by a mass spectrometer (HPR-20 QIC, Hiden Analytical) and, in parallel, by an infrared gas analyser (10E, Hartman und Braun). The MS data was quantitatively analysed, using the supplied software of the manufacturer (QGA Professional, Version 1.42i). The conversion curves measured in this way were Fourier filtered (Butterworth, normalised cut-off frequency: 10^{-6}, power: 60) to reduce their noise figure. It was checked and verified that relevant details, such as temporal trends and conversion levels, were not compromised in any way.

3. Results & discussion

3.1. Evaluation of the PFG NMR diffusion measurements

PFG NMR was used to measure the diffusivities of CO and CO_2 in npAu, being the relevant components for the oxidation of the former to the latter (CO + ½ O_2 -> CO_2) - a prototypical example of a reaction efficiently catalyzed by this material already at room temperature and below. In addition to these gases, CH_4 was included in the study for reference purposes. CH_4 molecules have a similar size than CO and CO_2 but, as far as adsorption and reaction on Au surfaces are concerned, CH_4 is expected to behave as an inert gas (see Introduction).

In a first step, the diffusivities of the bulk gases – i.e., in the absence of any npAu material in the NMR tube – were measured at a pressure of 15 bar. To this end, attenuation curves of the respective PFG NMR signals were recorded for all three gases, using diffusion times of 6 ms, 10 ms and 30 ms. As detailed in the supporting information (SI), on these grounds the molecular self-diffusion coefficients, compiled in Table 1, could be derived. Their comparison with reported experimental values obtained with other techniques under similar conditions as well as with theoretical values calculated on the basis of a refined ideal gas law description and the Chapman's and Enskog's approach reveals very good agreement in all cases, thus confirming the necessary sensitivity and precision of our PFG NMR measurements.

To determine the diffusivities within npAu's pore system, a sufficient number of npAu samples (see Experimental) was placed in the NMR tubes so that the measurement volume was filled to the maximum possible extent. Subsequently, the tubes were filled with CO, CO_2 or CH_4, respectively, at a pressure of 15 bar (in analogy to the experiments with the bulk gases) and then sealed. The results of the PFG NMR measurements obtained in the presence of the catalyst are presented in Fig. 1.

Except for long diffusion times (30 ms), in all cases – i.e., for all three gases – the attenuation curves recorded under these conditions clearly showed deviations from a mono-exponential decay as observed in the absence of npAu. Rather, the data could only be fitted, assuming a bi-exponential decay behavior (Eq. S3), in accord with two diffusing gas ensembles – one within the pores of the npAu specimen and one in the surrounding gas phase. The diffusivities derived for both ensembles are presented in Table 2. Within statistical uncertainty, the larger values (D_2) reflect the diffusion coefficients measured for the bulk gases (see above) and can thus be attributed to the molecules diffusing outside the material. As the other one (D_1) is smaller, it apparently must belong to the gas fraction diffusing inside npAu. The comparison of both values indicates that the transport within the pore system is only about half as fast as in the gas phase under identical conditions (pressure and temperature).

In the absence of strong gas-pore wall interactions (see Introduction) two factors contributing to the slower gas transport could play a role. The first one refers to onsetting Knudsen diffusion when applying pressures where the pore sizes are smaller than the mean free path of the diffusing gas molecules in the bulk gas phase. The second one results from the longer diffusion trajectories enforced by the pore system of the material specifically under consideration. For a pressure of 15 bar where the PFG NMR experiments were carried out, a calculation of the mean free path on the basis of kinetic gas theory reveals values below 10 nm for the molecules studied, i.e., values which are smaller than the typical mean pore diameters of npAu (18 nm ± 4.2 nm in case of the present study). Accordingly, a significant influence of Knudsen diffusion can be largely excluded under the applied experimental conditions, meaning that D_1 is expected to mostly reflect the second factor. Under these circumstances, the determined ratio D_2/D_1 directly corresponds to the tortuosity factor τ, introduced in the literature to quantify the diffusion resistance of a material as set by the shape and curvature as well as the lengths and connectivity of its pores.

In accordance with the similar size and weight of the molecules, alike values for the ratio of both diffusion constants were obtained for all three gases investigated (cf. Table 3). This finding corroborates the assumption of short surface residence times in case of CO and CO_2 (see Introduction) which, as reactants involved in the surface reaction studied, need to be accommodated on npAu's surface at least transiently, in contrast to CH_4. To furthermore verify the pressure independence of the results, additional experiments at 10 bars (where contributions from Knudsen diffusion should still be minor) were performed for CO_2 (see SI). Also, these measurements revealed, within statistical uncertainty, identical values D_2/D_1, thus assuring that the mean value of the ratio derived on the basis of the whole data set and amounting to 2.0 ± 0.2 indeed equals the (gas independent) tortuosity factor of npAu.

Aiming at a more differentiated understanding of the structural features influencing the diffusion of gases in porous materials, concepts have been proposed in the literature to split up τ, only integrally describing and quantifying this contribution to the decelerated mass transport, into two independent factors [38,39]:

Table 1
Self-diffusion coefficients of CO, CO_2 and CH_4 in the bulk gas phase, as derived from our PFG NMR measurements at 15 bar and 23 °C - in comparison to other experimental values reported in the literature for similar pressures and theoretical values, calculated according to Chapman and Enskog (incl. statistical uncertainties).

	This study		Other exp. Data[1]	Calculated[2]	
Gas	$D_{M,exp}$ ($\cdot 10^{-6}$) [m^2/s]	$\Delta D_{M,exp}$ ($\cdot 10^{-6}$) [m^2/s] (CI_{95})	$D_{M,lit}$ ($\cdot 10^{-6}$) [m^2/s]	$D_{M,calc}$ ($\cdot 10^{-6}$) [m^2/s]	$\Delta D_{M,calc}$ ($\cdot 10^{-6}$) [m^2/s]
CO	1.36	0.10	no data	1.41	0.04
CO_2	0.73	0.07	0.74[36]	0.78	0.04
CH_4	1.40	0.10	1.56[37]	1.56	0.03

[1] Data refers to 25 °C and 14.7 bar.
[2] Calculated on the basis of Chapman's and Enskog's theory with an expected validity for pressures up to 300 bar.

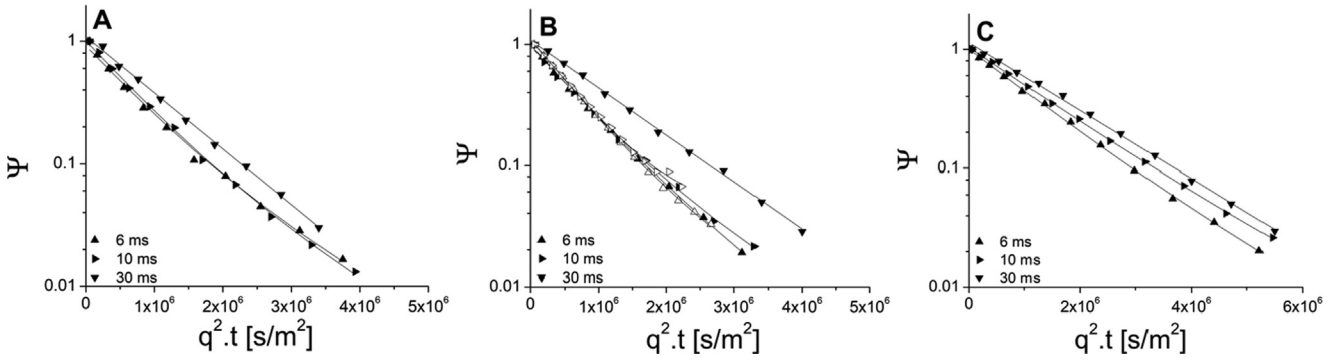

Fig. 1. ^{13}C PFG NMR attenuation curves measured for different diffusion times of CO (A), CH_4 (B), and CO_2 (C) at 23 °C and 15 bar in presence of the npAu samples. The corresponding data obtained for CH_4 diffusion by using ^1H PFG NMR (open symbols) are shown for comparison. The solid lines represent the results of the least-square fits based on a bi-exponential decay behavior (see SI for further details).

Table 2
Results of the least-square fitting of the data shown in Fig. 1, summarizing the root mean square displacements (RMSD) experienced by CO, CO_2 and CH_4 when diffusing inside (subscript: 1) and outside (subscript: 2) of the npAu material within the applied measurement time as well as the diffusion coefficients D_1 and D_2 derived on this basis. The last column shows their ratio D_2/D_1, representing the tortuosity factor τ.

t_D [ms]	Gas	$RMSD_1$ [μm]	$RMSD_2$ [μm]	D_1 ($\cdot 10^{-7}$) [m^2/s]	D_2 ($\cdot 10^{-7}$) [m^2/s]	D_2/D_1
6	CO	149 ± 15	218 ± 15	7.0 ± 1.4	15 ± 2	2.1 ± 0.5
10	CO	201 ± 20	290 ± 20	7.2 ± 1.4	15 ± 2	2.1 ± 0.4
30	CO	430 ± 20		10.5 ± 1		–
6	CH_4	167 ± 18	225 ± 15	8.8 ± 1.8	16 ± 2	1.8 ± 0.4
6*	CH_4	152 ± 16	228 ± 14	7.5 ± 1.5	17 ± 2	2.3 ± 0.5
10	CH_4	202 ± 22	299 ± 19	7.3 ± 1.5	16 ± 2	2.2 ± 0.5
10*	CH_4	193 ± 20	302 ± 19	6.8 ± 1.4	17 ± 2	2.5 ± 0.6
30	CH_4	397 ± 20		9.0 ± 0.9		–
6	CO_2	124 ± 13	167 ± 7	4.8 ± 1	8.75 ± 0.8	1.8 ± 0.4
10	CO_2	157 ± 17	208 ± 10	4.4 ± 0.9	7.8 ± 0.8	1.8 ± 0.4
30	CO_2	340 ± 19		6.6 ± 0.7		–

* Measurements done using ^1H PFG NMR.

Table 3
Average tortuosity factors of npAu derived from the ratio of the diffusivities of CO, CO_2 and CH_4 outside and inside npAu on the basis of the data shown in Table 2.

Sorbate	Pressure/bar	Average tortuosity factor τ
CO	15	2.1 ± 0.4
CH_4	15	2.2 ± 0.3
CO_2	15	1.8 ± 0.3
CO_2	10	1.8 ± 0.4

- impediments due to varying pore diameters, possibly resulting in "bottle necks" for the diffusing molecules;
- elongation of the diffusive pathways due to non-straight but meandering pores.

As a measure for the first contribution, a parameter called *constrictivity* δ was introduced in the literature, whereas contributions of the latter kind were subsumed in a quantity, (unfortunately) also called *tortuosity* and, for the sake of clarity, denoted τ' in the following. The integral tortuosity τ, as determined by PGF NMR and dealt with above, is then related to δ and τ' in the following way [38,39]:

$$\tau = \frac{\tau'^2}{\delta} \quad (1)$$

The constrictivity δ of a pore system can usually comparatively easily assessed on the basis of a microscopic evaluation of the pore diameters (via SEM or TEM, for instance) [39]. For npAu such an analysis based on the width of its pore size distribution, which was shown to be independent of the mean diameter if normalized to it, yields a value of δ = 0.54, as detailed in section 3 of the SI. Using this value and the value for τ (2.0) derived from the PFG NMR measurements, Eq. (1) indicates that τ' is close to 1 (1.1),

implying comparatively small contributions due to pathway elongations enforced by npAu's pore system. Rather, the main effect seems to result from pore diameter variations in case of this material.

3.2. Determination of diffusivities under catalytic conditions

Knowing npAu's tortuosity τ as the material specific parameter governing the diffusive mass transport within its porous system enables quantitatively assessing its influence on the conversion levels achievable under the catalytic reaction conditions applied. In this context, it has to be considered, however, that CO oxidation over npAu was typically studied under significantly lower pressures (1 bar) than those employed for the PFG NMR experiments and that gas mixtures (and not pure gases) are present under catalytic conditions. To this end, the molecular diffusion coefficients D_M of the reactants first need to be rescaled to 1 bar. On this basis, the corresponding values in the applied gas mixture $D_{M,mix}$ can be calculated. To include potential contributions of Knudsen diffusion (D_K, see eq. S9 in the SI), which are likely to play a significant role for mesoporous materials, such as npAu, around 1 bar, finally the total diffusion coefficient $D_{T,mix}$ has to be determined (eq. S8 in the SI). For CO, CO_2, O_2 and He (carrier gas), i.e., the gases comprising the feed for the catalytic experiments described in the next subsection, the corresponding values are compiled in Table 4. (All details necessary for their assessment can be found in section 4 of the SI.) Comparing $D_{T,mix}$ and D_K, it becomes apparent that they are very similar in all cases. This equality underpins that, indeed, Knudsen diffusion dominates the mass transport in npAu at 1 bar – meaning that its pore diameters are distinctly smaller than the mean free path of the molecules in the bulk gas phase under these conditions.

Under these circumstances, it can be safely assumed that transport and self-diffusion coefficients are identical and that effective diffusivities D_E relevant for the diffusive mass transport in the pore system under reaction conditions can be calculated according to [16,24,40]:

$$D_{E,i} = \frac{\phi}{\tau} \cdot D_{T,mix,i} \tag{2}$$

Here, not only the determined tortuosity factor τ but also the known porosity ϕ of npAu (0.7) has to be taken into account. As expected, very similar values are obtained in this way for all gases - except for He as a distinctly lighter gas (yet, as the carrier gas, not involved in the reaction): $0.83–1.03 \cdot 10^{-6}$ m/s^2.

3.3. CO oxidation over npAu and determination of the microkinetics

It was already mentioned in the Introduction that previous work on low-temperature CO oxidation over npAu suggested that it is the supply of CO that controls and limits its catalytic turnover on the surface so that a rate law of first order can be applied to describe its microkinetics [12]:

$$r_{int} = k \cdot c_{CO} = k \cdot \frac{p_{CO}}{R \cdot T} \tag{3}$$

c_{CO}: CO concentration; p_{CO}: CO partial pressure.

For a porous catalyst, the level of conversion actually observed usually is diminished as a consequence of a retarded supply of the reactants to its inner sections by diffusive mass transport. The effectiveness factor of the catalytic process η is then defined as the ratio of the macroscopically observed rate r_{obs} and the microkinetic rate r_{int}:

$$\eta = \frac{r_{obs}}{r_{int}} \Longleftrightarrow r_{obs} = \eta \cdot r_{int} \tag{4}$$

On one hand, η is dependent on the macroscopic shape and size of the catalyst particles, pellets, or monoliths used. On the other hand, the relationship between the microkinetic rate and the diffusive flux through the catalyst's pores is decisive. All these quantities can be merged into a single one, called Thiele Modulus, constituting the parameter which determines the effectiveness factor η achievable under the applied process conditions. For a microkinetic rate law of 1st order the Thiele Modulus φ has the following form [43]:

$$\varphi = \sqrt{\frac{k \cdot \ell^2}{D_E}} \tag{5}$$

and is connected to η as follows:

$$\eta = \frac{\tanh(\varphi)}{\varphi} \tag{6}$$

Here, D_E refers to the effective diffusivity of the kinetically relevant reactant within the pore system, i.e., in our case to CO (see Table 4: $D_E = 1.03 \cdot 10^{-6}$ m^2/s) and ℓ to the so-called characteristic length, representing a 1D measure for the distances to be overcome by diffusion within the applied catalyst particles. As detailed in the SI, this quantity can be calculated on the basis of their shape and size and equals in case of thin, disc-shaped specimen as given for the npAu monoliths (diameter: 5 mm, thickness: 200 μm) employed in this study to half of their thickness (100 μm).

A representative progression of the conversion of CO to CO_2 as achieved with such monolithic samples at 30 °C after applying an activation protocol which was previously reported to ensure maximal catalytic turnover is shown in Fig. 2 (lower trace). As inferred from the figure, the maximum conversion eventually reached amounts to X = ~40 % which, if transformed into a CO_2 formation rate (r_{obs}), corresponds to the macrokinetics under the given conditions. As elucidated in more detail in the SI, on this basis and the experimentally determined transport properties of npAu the microkinetic rate constants k (referred to the volume) and k_A (referred to the catalyst surface area) as well as the corresponding turnover frequency (TOF: number of CO molecules reacted to CO_2 per surface atom and second) can be straightforwardly calculated. The results are summarized in Table 5.

When comparing the TOF derived in this way with values previously reported in the literature, it is important to note that, in contrast to k and k_A, this measure for the catalytic activity is proportional to the CO concentration or partial pressure, respectively, because it corresponds to a rate (expressed in microscopic terms) and not to a rate constant. As shown in Ref. [12], the CO_2 formation rate increases, under conditions of O_2 excess, linearly up to several 10 vol% (in line with a rate law of 1st order) so that at higher CO partial pressures significantly higher TOFs can be reached. In Table S2 a synopsis of kinetic results that have been published on low-temperature CO oxidation over npAu since 2006 is presented. When considering the CO concentrations applied there and relating the reported TOFs to 1 vol% CO for example, (as used here) it turns out that, by trend, the values are smaller than the one determined in this study. This finding, however, is not unexpected. While a varying and unknown degree of mass transport limitations is one likely reason for the scatter, also an incomplete activation of the npAu catalysts might be another one.

Having access to the diffusive transport properties of npAu and being able to seize best-possible conversion levels reproducibly, such ambiguities, however, can be overcome. Furthermore, predictions regarding an optimized catalyst shape can be made. On the basis of the Thiele Modulus for the npAu discs a catalyst effectiveness factor η = 0.68 is calculated, indicating that in this case mass transport still plays a major role, which limits the catalytic activity

Table 4
Molecular (D_M) and calculated Knudsen (D_K) diffusion coefficients as well as the molecular ($D_{M,mix}$) and resulting total diffusion coefficients ($D_{T,mix}$) in the reaction mixture for all gases used for studying CO oxidation over npAu at 1 bar and 30 °C. On the basis of $D_{T,mix}$ and the tortuosity determined for npAu by PFG NMR, effective diffusion coefficients D_E relevant for the mass transport within the pore system were calculated and are given in the last column.

Gas	D_M ($\cdot 10^{-6}$) [m^2/s]	$D_{M,Mix}$ ($\cdot 10^{-6}$) [m^2/s]	D_K ($\cdot 10^{-6}$) [m^2/s][2]	$D_{T,Mix}$ ($\cdot 10^{-6}$) [m^2/s]	D_E ($\cdot 10^{-6}$) [m^2/s]
CO	20.4	83.84	3.19	3.07	1.03
O_2	22.12[1]	106.91	2.99	2.90	0.97
CO_2	11.0	70.03	2.55	2.46	0.83
He*	176.38[1]	109.27	8.44	7.84	2.63

[1] Calculated on the basis of Chapman and Enskog's theory [17,41,42].
[2] Calculated on the basis of kinetic gas theory: see SI.
* Carrier gas.

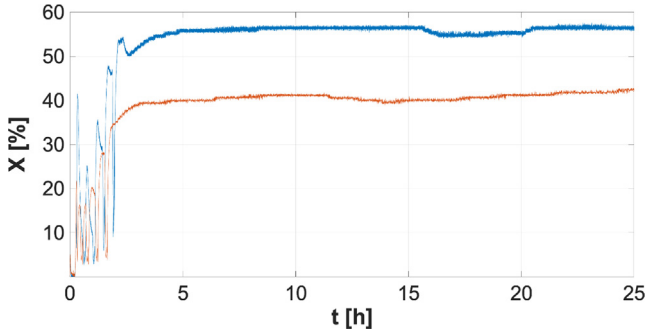

Fig. 2. Evolution of catalytic conversion X of CO to CO_2 as observed for different types of npAu catalysts at 30 °C after activating them on the basis of a protocol reported previously (resulting in the oscillatory behavior recorded between 0 and 2.5 h). Lower trace: monolithic npAu discs (5 mm diameter and 200 μm thickness); upper trace: npAu platelets exhibiting the same thickness but diameters in the range of just a few 100 μm.

to about 2/3 as compared to npAu's full potential. As inferred from Fig. 3, a reduction of the characteristic length l to already a third (i.e., to < 33 μm) should lead to an increase of η to 0.95 or even higher. As detailed in the SI, such a situation is reached, when decreasing the disc diameter to the dimension of the disc height (200 μm), turning ℓ from h/2 to h/6.

To verify this prediction, we developed a simple method of breaking up the monolithic npAu samples into smaller pieces, without compromising the accessibility of the pore system (see Experimental). In this way, we could successfully transform the discs into platelets with diameters in the range of just a few 100 μm (even though exhibiting a broad size range). Repeating the catalytic experiments with this form of the catalyst (under otherwise identical reaction conditions), an increase of the conversion level by ~45–50% (corresponding to absolute conversions of 55–60% under the given experimental conditions) could indeed be achieved (see Fig. 2, upper trace). Based on the microkinetic rate constant k, this corresponds to a catalyst effectiveness factor η larger than 95%, in agreement with the expectation based on the smaller particles size.

4. Conclusions

For the first time, we succeeded to measure diffusivities of gas molecules in a porous metallic material by PFG NMR. The system we investigated, nanoporous gold, represents an interesting heterogeneous catalyst which has been found to efficiently catalyze total and partial aerobic oxidation reactions with high activities and selectivities already at room temperature. Taking CO oxidation as an example for which the diffusion of the reactants CO and CO_2 can be straightforwardly studied by ^{13}C PFG NMR, we were able to experimentally assess the impediment set by the pore system of npAu for their diffusive transport. By including CH_4 as an inert molecule in the experiments, showing the same tortuosity as the two other gases, it was assured that chemisorption of the reactants on the pore walls – being the necessary condition for catalytic conversion - does not influence the data. On grounds of the PFG NMR results, the tortuosity of npAu's pore system could be determined, revealing that mass transport in the material is slowed down by a factor of ~2 as compared to the bulk gas phase. This value is in general agreement with theoretical predictions for porous systems exhibiting high porosities [44,45].

Owing to the independent characterization of the transport properties, we were able to disentangle the macrokinetics, i.e., the observed CO_2 formation rate, and the microkinetics, characterizing the genuine catalytic potential of npAu with respect to this reaction. The turnover frequency determined partly excels previously reported values in the literature, suggesting influences of diffusive transport limitations in former studies. For thin monolithic npAu discs, for instance, typically employed for catalytic investigations in the past, diameters of several mm and a thickness of 200 μm already reduce the catalytic effectiveness by about a third.

Having experimentally determined the microkinetics, this knowledge allowed us making predictions for more efficient shapes of the catalyst where transport limitations are minimized. Making a first attempt into this direction, we broke up larger npAu discs into smaller platelets. The reduction of the catalyst lateral size to values in the range of a few 100 μm resulted in an increase of the catalytic conversion of CO to CO_2 by about 50 % which, in

Table 5
Micro- and macrokinetics of low-temperature CO oxidation over nanoporous gold: rate constant per volume (k) and per area catalyst (k_A), turnover frequency (TOF) as well as catalyst effectiveness factor η for large monolithic npAu discs with a thickness of 200 μm and a diameter of 5 mm as well as for smaller npAu platelets where both, thickness and lateral dimensions, were in the range of 200 μm.

Microkinetics and macrokinetics of CO oxidation over npAu at 30 °C and 1 bar				
Microkinetics			Macrokinetics: catalyst effectiveness factor η	
			npAu discs (h = 200 μm, d = 5 mm → ℓ = 100 μm)	npAu platelets (h = 200 μm, d = 200 μm → ℓ = 33.3μm)
k (1/s)	k_A (m/s)	TOF (1/s)	0.68 (φ = 1.23)	0.97 = **1.43** · η_{discs} (φ = 0.34)
155	$1.76 \cdot 10^{-6}$	0.03		

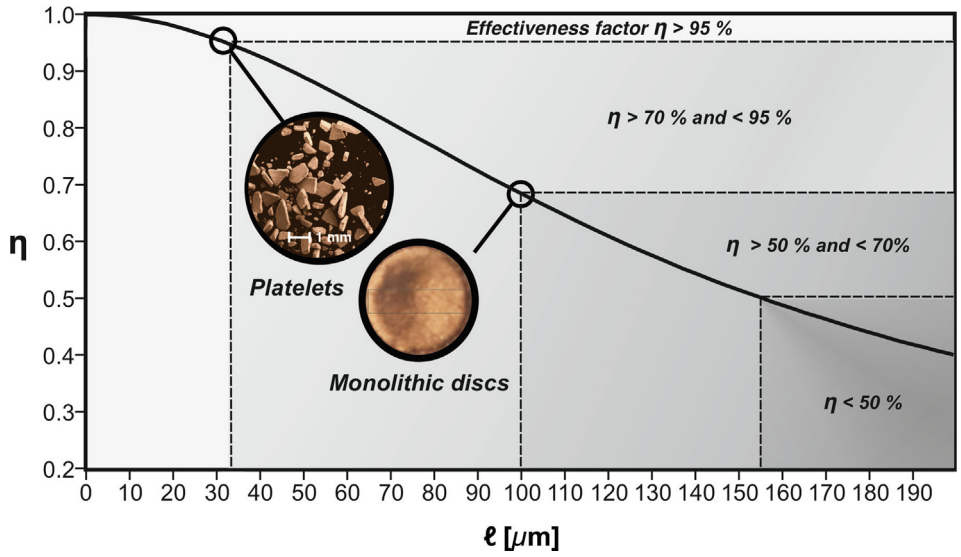

Fig. 3. Effectiveness factor η of npAu catalysts exhibiting different shapes and characteristic lengths.

agreement with predictions, corresponds to an improvement of the effectiveness factor η to almost 100%.

An option for a more controlled fabrication of size-selected npAu particles by breaking up larger npAu monoliths is given by tailoring its gain structure during preparation, since fracture predominantly occurs at grain boundaries. On the one hand, it has been shown that the grain sizes of the starting alloy are conserved during the dealloying process [46]. On the other hand, it is well-established metallurgic knowledge how grain sizes of cold rolled metals change and can be influenced by intermittent annealing steps [47,48]. Thus, optimizing the protocols for thinning and treating the starting alloy used for the dealloying is expected to represent a viable way for preparing npAu catalysts which are optimized with respect to their diffusive transport properties so that their catalytic potential can be fully exploited. An alternative, requiring, however, much more sophisticated fabrication approaches, are hieratically designed nanoporous structures, additionally providing macroporous transport capabilities as have also been suggested in the literature [8,15].

Data availability

Data will be made available on request.

Acknowledgements

M.B. and T.R. acknowledge gratefully funding of the work provided by the German Research Foundation (DFG) within the framework of the Research Unit 2213 "Nanoporous Gold" (grand no.: BA 1710/29-2 and RI 1025/3-2). A portion of this work was carried out in the McKnight Brain Institute at the National High Magnetic Field Laboratory's AMRIS Facility, which is supported by National Science Foundation Cooperative Agreement No. DMR-1157490 and the State of Florida. This work was supported in part by an NIH award, S10RR031637, for magnetic resonance instrumentation.

Appendix A. Supplementary material

Supplementary data to this article can be found online at https://doi.org/10.1016/j.jcat.2022.08.020.

References

[1] C. Xu, J. Su, X. Xu, P. Liu, H. Zhao, F. Tian, Y. Ding, Low temperature CO oxidation over unsupported nanoporous gold, J. Am. Chem. Soc. 129 (2007) 42–43, https://doi.org/10.1021/ja0675503.
[2] V. Zielasek, B. Jürgens, C. Schulz, J. Biener, M.M. Biener, A.V. Hamza, M. Bäumer, Gold catalysts: nanoporous gold foams, Angew. Chem. – Int. Ed. 45 (2006) 8241–8244, https://doi.org/10.1002/anie.200602484.
[3] A. Wittstock, J. Biener, J. Erlebacher, M. Bäumer, Nanoporous Gold: From an Ancient Technology to a High-tech Material, Royal Society of Chemistry (RSC Nanoscience & Nanotechnology, vol. 22), Cambridge, 2012, ISBN 978-1-84973-374-8. <https://doi.org/10.1039/9781849735285>.
[4] A. Wittstock, V. Zielasek, J. Biener, C.M. Friend, M. Bäumer, Nanoporous gold catalysts for selective methanol at low temperature, Science 327 (2008) 319–323.
[5] M. Haruta, Novel catalysis of gold deposited on metal oxides, CATTECH 6 (2002) 102–115, https://doi.org/10.1023/A:1020181423055.
[6] I. McCue, J. Stuckner, M. Murayama, M.J. Demkowicz, Gaining new insights into nanoporous gold by mining and analysis of published images, Sci. Rep. 8 (2018) 1–11, https://doi.org/10.1038/s41598-018-25122-3.
[7] A. Wittstock, J. Biener, M. Bäumer, Nanoporous gold: a new material for catalytic and sensor applications, Phys. Chem. Chem. Phys. 12 (2010) 12919–12930, https://doi.org/10.1039/c0cp00757a.
[8] J.D. Lee, J.B. Miller, A.V. Shneidman, L. Sun, J.F. Weaver, J. Aizenberg, J. Biener, J. A. Boscoboinik, A.C. Foucher, A.I. Frenkel, J.E.S. van der Hoeven, B. Kozinsky, N. Marcella, M.M. Montemore, H.T. Ngan, C.R. O'Connor, C.J. Owen, D.J. Stacchiola, E.A. Stach, R.J. Madix, P. Sautet, C.M. Friend, Dilute alloys based on Au, Ag, or Cu for efficient catalysis: from synthesis to active sites, Chem. Rev. 122 (9) (2022) 8758–8808.
[9] L.V. Moskaleva, S. Röhe, A. Wittstock, V. Zielasek, T. Klüner, K.M. Neyman, M. Bäumer, Silver residues as a possible key to a remarkable oxidative catalytic activity of nanoporous gold, Phys. Chem. Chem. Phys. 13 (2011) 4529–4539, https://doi.org/10.1039/c0cp02372h.
[10] W. Dononelli, G. Tomaschun, T. Klüner, L.V. Moskaleva, Understanding oxygen activation on nanoporous gold, ACS Catal. 9 (2019) 5204–5216, https://doi.org/10.1021/acscatal.9b00682.
[11] G. Pia, E. Sogne, A. Falqui, F. Delogu, Ag surface segregation in nanoporous Au catalysts during CO oxidation, Sci. Rep. 8 (2018) 1–9, https://doi.org/10.1038/s41598-018-33631-4.
[12] A. Wittstock, B. Neumann, A. Schaefer, K. Dumbuya, C. Kübel, M.M. Biener, V. Zielasek, H.P. Steinrück, J.M. Gottfried, J. Biener, A. Hamza, M. Bäumer, Nanoporous Au: an unsupported pure gold catalyst?, J Phys. Chem. C. 113 (2009) 5593–5600, https://doi.org/10.1021/jp808185v.
[13] L.C. Wang, Y. Zhong, D. Widmann, J. Weissmüller, R.J. Behm, On the role of residual Ag in nanoporous Au catalysts for CO oxidation: a combined microreactor and TAP reactor study, ChemCatChem 4 (2012) 251–259, https://doi.org/10.1002/cctc.201100297.
[14] S. Wild, M. Bäumer, T. Risse, Thermal activation of nanoporous gold for carbon monoxide oxidation, J. Phys. Chem. C. 126 (2022) 1770–1777, https://doi.org/10.1021/acs.jpcc.1c08222.
[15] M.L. Personick, B. Zugic, M.M. Biener, J. Biener, R.J. Madix, C.M. Friend, Ozone-activated nanoporous gold: a stable and storable material for catalytic oxidation, ACS Catal. 5 (2015) 4237–4241, https://doi.org/10.1021/acscatal.5b00330.

[16] J. Kärger, D.M. Ruthven, D.N. Theodorou (Eds.), Diffusion in Nanoporous Materials, Wiley, 2012.
[17] J.O. Hirschfelder, C.F. Curtiss, R.B. Bird, Molecular Theory of Gases and Liquids, Wiley & Sons Ltd, 1954.
[18] J. Kärger, S. Vasenkov, Quantitation of diffusion in zeolite catalysts, Micropor. Mesopor. Mater. 85 (2005) 195–206, https://doi.org/10.1016/j.micromeso.2005.06.020.
[19] S.J. Cooper, A. Bertei, P.R. Shearing, J.A. Kilner, N.P. Brandon, TauFactor: an open-source application for calculating tortuosity factors from tomographic data, SoftwareX 5 (2016) 203–210, https://doi.org/10.1016/j.softx.2016.09.002.
[20] R. Mueller, S. Zhang, M. Klink, M. Bäumer, S. Vasenkov, The origin of a large apparent tortuosity factor for the Knudsen diffusion inside monoliths of a samaria-alumina aerogel catalyst: a diffusion NMR study, Phys. Chem. Chem. Phys. 17 (2015) 27481–27487, https://doi.org/10.1039/c5cp04609b.
[21] J. Kärger, M. Avramovska, D. Freude, J. Haase, S. Hwang, R. Valiullin, Pulsed field gradient NMR diffusion measurement in nanoporous materials, Adsorption 27 (2021) 453–484, https://doi.org/10.1007/s10450-020-00290-9.
[22] C. D'Agostino, R.D. Armstrong, G.J. Hutchings, L.F. Gladden, Product inhibition in glycerol oxidation over Au/TiO2 catalysts quantified by NMR relaxation, ACS Catal. 8 (2018) 7334–7339, https://doi.org/10.1021/acscatal.8b01516.
[23] C. D'Agostino, Y. Ryabenkova, P.J. Miedziak, S.H. Taylor, G.J. Hutchings, L.F. Gladden, M.D. Mantle, Deactivation studies of a carbon supported AuPt nanoparticulate catalyst in the liquid-phase aerobic oxidation of 1,2-propanediol, Catal, Sci. Technol. 4 (2014) 1313–1322, https://doi.org/10.1039/c4cy00027g.
[24] M.D. Mantle, D.I. Enache, E. Nowicka, S.P. Davies, J.K. Edwards, C. Dagostino, D. P. Mascarenhas, L. Durham, M. Sankar, D.W. Knight, L.F. Gladden, S.H. Taylor, G.J. Hutchings, Pulsed-field gradient NMR spectroscopic studies of alcohols in supported gold catalysts, J. Phys. Chem. C. 115 (2011) 1073–1079, https://doi.org/10.1021/jp105946q.
[25] N. Lopez, J.K. Nørskov, Catalytic CO oxidation by a gold nanoparticle: a density functional study, J. Am. Chem. Soc. 124 (2002) 11262–11263, https://doi.org/10.1021/ja026998a.
[26] S. Röhe, K. Frank, A. Schaefer, A. Wittstock, V. Zielasek, A. Rosenauer, M. Bäumer, CO oxidation on nanoporous gold: a combined TPD and XPS study of active catalysts, Surf. Sci. 609 (2013) 106–112, https://doi.org/10.1016/j.susc.2012.11.011.
[27] M. Mavrikakis, P. Stoltze, J.K. Nørskov, Making gold less noble, Catal. Letters. 64 (2000) 101–106.
[28] A. Lackmann, C. Mahr, M. Schowalter, L. Fitzek, J. Weissmüller, A. Rosenauer, A. Wittstock, A comparative study of alcohol oxidation over nanoporous gold in gas and liquid phase, J. Catal. 353 (2017) 99–106, https://doi.org/10.1016/j.jcat.2017.07.008.
[29] W.L. Yim, T. Nowitzki, M. Necke, H. Schnars, P. Nickut, J. Biener, M.M. Biener, V. Zielasek, K. Al-Shamery, T. Klüner, M. Bäumer, Universal phenomena of CO adsorption on gold surfaces with low-coordinated sites, J. Phys. Chem. C. 111 (2007) 445–451, https://doi.org/10.1021/jp0665729.
[30] A.P. Farkas, F. Solymosi, Activation and reactions of CO_2 on a K-promoted Au (111) surface, J. Phys. Chem. C. 113 (2009) 19930–19936, https://doi.org/10.1021/jp9061779.
[31] C. Xu, X. Xu, J. Su, Y. Ding, Research on unsupported nanoporous gold catalyst for CO oxidation, J. Catal. 252 (2007) 243–248, https://doi.org/10.1016/j.jcat.2007.09.016.
[32] E.W. Thiele, Relation between catalytic activity and size of particle, Ind. Eng. Chem. 31 (1939) 916–920, https://doi.org/10.1021/ie50355a027.
[33] D. Steinebrunner, G. Schnurpfeil, A. Wichmann, D. Wöhrle, A. Wittstock, Synergistic effect in zinc phthalocyanine—nanoporous gold hybrid materials for enhanced photocatalytic oxidations, Catalysts 9 (2019) 555, https://doi.org/10.3390/catal9060555.
[34] M. Dvoyashkin, J. Zang, G.I. Yucelen, A. Katihar, S. Nair, D.S. Sholl, C.R. Bowers, S. Vasenkov, Diffusion of tetrafluoromethane in single-walled aluminosilicate nanotubes: pulsed field gradient NMR and molecular dynamics simulations, J. Phys. Chem. C. 116 (2012) 21350–21355, https://doi.org/10.1021/jp3054247.
[35] R.M. Corns, M.J.R. Hoch, T. Sun, J.T. Markert, Pulsed field gradient stimulated echo methods for improved NMR diffusion measurements in heterogeneous systems, J. Magn. Reson. 83 (1989) 252–266, https://doi.org/10.1016/0022-2364(89)90189-3.
[36] S. Takahashi, H. Iwasaki, The diffusion of gases at high pressures. i. the self-diffusion coefficient of carbon dioxide, Bull. Chem. Soc. Jpn. 39 (1966) 2105–2109, https://doi.org/10.1246/bcsj.39.2105.
[37] N.J. Trappeniers, P.H. Oosting, Selfdiffusion in gaseous and liquid methane, Phys. Lett. 23 (1966) 445–447, https://doi.org/10.1016/0031-9163(66)91086-9.
[38] J. van Brakel, P.M. Heertjes, Analysis of diffusion in macroporous media in terms of a porosity, a tortuosity and a constrictivity factor, Int. J. Heat Mass Transf. 17 (1974) 1093–1103, https://doi.org/10.1016/0017-9310(74)90190-2.
[39] E.E. Petersen, Diffusion in a pore of varying cross section, AIChE J. 4 (1958) 343–345, https://doi.org/10.1002/aic.690040322.
[40] C. D'Agostino, J. Mitchell, L.F. Gladden, M.D. Mantle, Hydrogen bonding network disruption in mesoporous catalyst supports probed by PFG-NMR diffusometry and NMR relaxometry, J. Phys. Chem. C. 116 (2012) 8975–8982, https://doi.org/10.1021/jp2123295.
[41] M.J. Slaman, R.A. Aziz, Accurate transport properties and second virial coefficients for helium based on a state-of-the art interatomic potential, Int. J. Thermophys. 16 (4) (1995) 1029.
[42] A. Boushehri, J. Bzowski, J. Kestin, E.A. Mason, Equilibrium and transport properties of eleven polyatomic gases at low density, J. Phys. Chem. Ref. Data. 16 (3) (1987) 445–466.
[43] G. Emig, E. Klemm, Technische Chemie, in: Tech. Chemie, fifth ed., Springer, 2005, pp. 24–25.
[44] M. Barrande, R. Bouchet, R. Denoyel, Tortuosity of porous particles, Anal. Chem. 79 (2007) 9115–9121, https://doi.org/10.1021/ac071377r.
[45] Z. Sun, X. Tang, G. Cheng, Numerical simulation for tortuosity of porous media, Micropor. Mesopor. Mater. 173 (2013) 37–42, https://doi.org/10.1016/j.micromeso.2013.01.035.
[46] Z. Qi, U. Vainio, A. Kornowski, M. Ritter, H. Weller, H. Jin, J. Weissmüller, Porous gold with a nested-network architecture and ultrafine structure, Adv. Funct. Mater. 25 (2015) 2530–2536, https://doi.org/10.1002/adfm.201404544.
[47] H. Hui, R. Xia, J. Li, Q. Mei, Y. Ma, F. Chen, Y. Lei, Effects of cold rolling and annealing prior to dealloying on the microstructure of nanoporous gold, Nanomaterials. 8 (2018) 540, https://doi.org/10.3390/nano8070540.
[48] J.H. Cho, H.P. Ha, K.H. Oh, Recrystallization and grain growth of cold-rolled gold sheet, Metall. Mater. Trans. 36 (2005) 3415–3425, https://doi.org/10.1007/s11661-005-0015-5.